SUPPORTING INFORMATION

A HNO_3-responsive aqueous biphasic system for metal separation: application towards Ce^{IV} recovery

Nicolas Schaeffer,[a,*] Silvia J.R. Vargas,[a] Helena Passos,[a] Paula Brandão,[a] Helena I.S. Nogueira,[a] Lenka Svecova,[b] Nicolas Papaiconomou,[c] João A.P. Coutinho[a]

[a] *CICECO, Aveiro Institute of Materials, Department of Chemistry, University of Aveiro, 3810-193 Aveiro, Portugal.*

[b] *Univ. Grenoble Alpes, Univ. Savoie Mont Blanc, CNRS, Grenoble INP, LEPMI, 38000 Grenoble, France*

[c] *Institut de Chimie de Nice, 28 avenue Valrose, Université Côte d'Azur, 06108, Nice, France*

* Corresponding author: nicolas.schaeffer@ua.pt

Number of pages – 19

Number of figures – 10

Number of Tables - 7

Methodology

Materials and instrumentation

Materials

The acidic aqueous biphasic systems (AcABS) studied in this work were established by various aqueous solutions of HNO_3 (65.0 wt.% from Sigma-Aldrich) with $[N_{4444}][NO_3]$ or $[N_{4444}]Cl$ (97.0 wt.% from Sigma-Aldrich). The list of metal salts used, including their purity and supplier, is available in **Table S5**. All chemicals were used as received without further purification. Ultrapure, double distilled water, passed through a reverse osmosis system and further treated with a Milli-Q plus 185 water purification apparatus, (18.2 MΩ.cm at 25 °C) was used for all experiments.

Raman spectroscopy

Raman spectra were acquired on a Bruker MultiRAM equipped with a 1064 nm Nd-YAG laser source and a nitrogen cooled germanium detector. All spectra were recorded in the 3600 to 100 cm^{-1} range with a resolution of 4 cm^{-1}. For solid samples, 200 scans and a laser power of 100 mW were used whilst 350 mW and 400 scans were applied for liquid samples. The obtained spectra were deconvoluted using the Origin software package. The baseline was fitted using an exponential decay function and subtracted. The resulting area was deconvoluted into Gaussian components.

Nuclear magnetic resonance (NMR) spectroscopy

A Bruker Avance 300 operating at 75 MHz was used to perform both qualitative and quantitative ^{1}H-NMR analysis at 293 K of aqueous $[N_{4444}][NO_3]$ solutions with deuterated water (D2O) as the solvent and tetramethylsilane as the reference. Quantitative ^{1}H-NMR analysis was performed with benzene as internal standard placed in a coaxial insert to quantify the concentration of $[N_{4444}][NO_3]$ in the AcABS bottom phase as a function of HNO_3 concentration.

Powder X-ray diffraction (PXRD)

PXRD was determined using a Bruker AXS with Cu Kα radiation operating at 45 kV and a spinning discs sample holder. Diffractograms were analysed using the X'pert Highscore Plus software package and the patterns matched against those in the International Centre for Diffraction Data (ICDD) database.

Single crystal X-ray diffraction (PXRD)

Single crystal X-ray diffraction of the orange precipitate formed at high Ce^{IV} to $[N_{4444}][NO_3]$ loading was collected at low temperature (150 K) with monochromated Mo-Kα radiation (λ = 0.71073 Å) on a Bruker Kappa APEX II diffractometer equipped with a CCD area detector. Data reduction was carried out using the SAINT-Plus software package.[1] Multi-scan absorption correction was applied to all intensity data using the SADABS program.[2] The structure was refined via full matrix least squares on F2 using the SHELX-2014 suite.[3] All non-hydrogen atoms were refined with anisotropic thermal parameters. The C-H hydrogen atoms were included in the structure factor calculations in geometrically idealized positions with isotropic thermal displacements depending on the parent atom, using a riding model. Molecular diagrams were drawn with the Mercury 4.0 software.[4] The Crystal data and selected refinement details are listed in **Table S6**. The structures were deposited with the Cambridge Crystallographic Data Centre with the number 2081287.

Scanning electron microscopy (SEM)

Sample morphology was analysed by scanning electron microscopy (SEM) with energy-dispersive X-ray spectroscopy (EDS) using a Hitachi S4100 microscope after carbon sputter-coating.

Aggregate size determination

Aggregate size measurements of 20.0 wt.% IL in varying concentration of HNO_3 at 293 K were made by dynamic light scattering (DLS) (Malvern Zetasizer Nano-ZS). Samples were irradiated with red light (a HeNe laser, a wavelength of 565 nm) and the intensity fluctuations of the scattered light were detected at a backscattering angle of 173° to generate an autocorrelation function. The cumulant analysis of this function provided by software DTS v 7.03 yielded the particle size and the distribution width.

Metal Quantification

Metal quantification in both the IL-rich and bottom phase of the AcABS was performed using a Picofox S2 (Bruker Nano (Billerica, MA, USA)) total reflection X-ray fluorescence spectrometer with a molybdenum X-ray source. The voltage of the X-ray tube was 50 kV and the current 600 μA. All carriers were first pre-treated with 10 μL of silicon in isopropanol solution and dried at 353 K for 30 min. Samples were diluted in 1.0 wt.% polyvinyl alcohol acidified at pH = 1.0 using HCl and spiked with a known concentration of $GaCl_3$ for REEs

containing samples of YCl_3 for all other samples to obtain a final standard element concentration of 5 to 30 ppm (depending on the sample metal content). Ten microliters of each solution containing the metals and standard of Ga were added onto a clean carrier and dried on a hot plate at 353 K for 15 min.

Figures

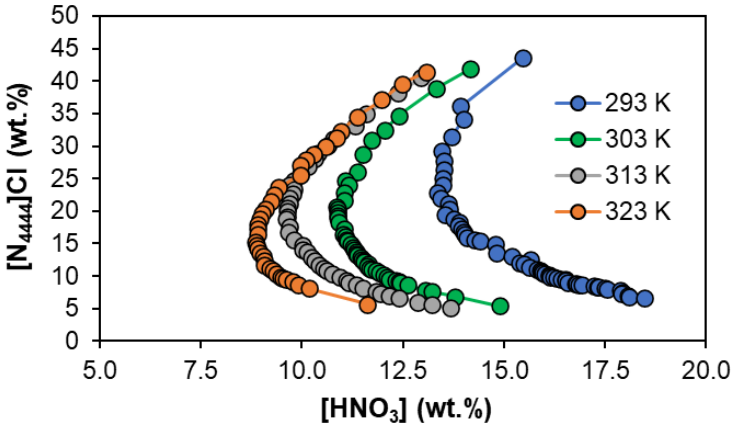

Figure S1. Phase diagram of the $[N_{4444}]Cl + HNO_3 + H_2O$ system as a function of temperature.

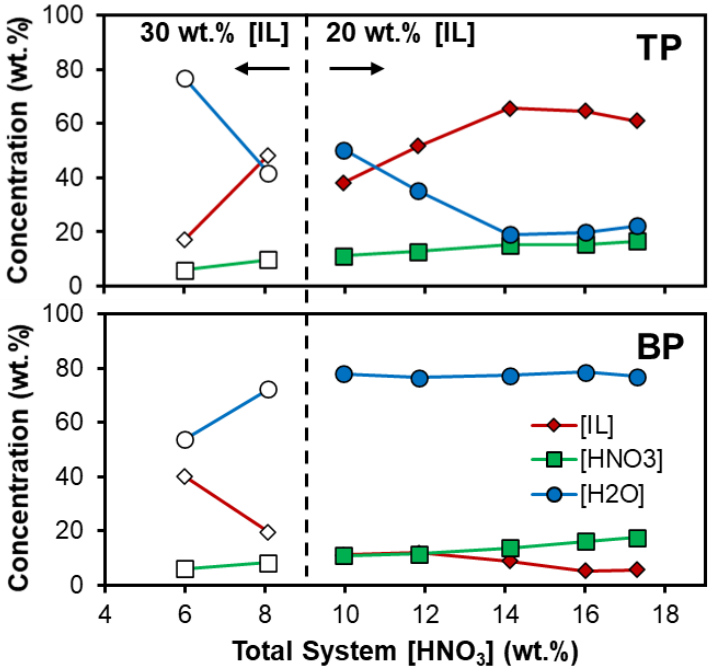

Figure S2. Experimental top phase (TP) and bottom phase (BP) composition in the $[N_{4444}][NO_3] + HNO_3 + H_2O$ AcABS as a function of HNO_3 concentration. H_2O concentration in the BP was determined by mass balance. The IL concentration was increased at lower HNO_3 concentration to address the small volume of the IL-rich phase which resulted in significant experimental errors.

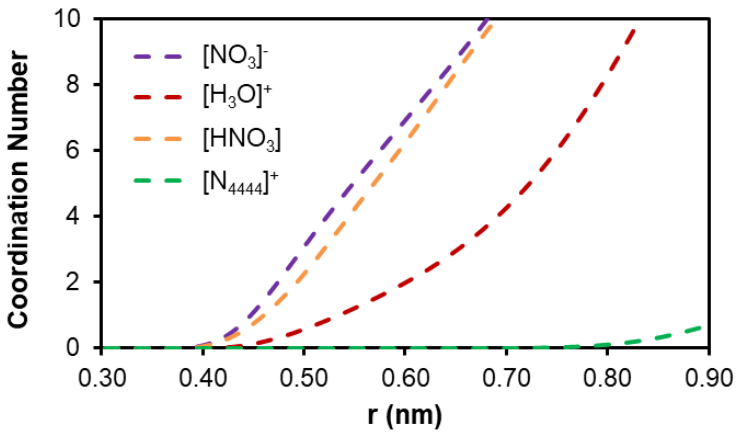

Figure S3. Derived coordination number from the radial distribution functions between the central nitrogen atom of $[N_{4444}]^+$ and the other species presented in Figure 1D of the manuscript. [IL]=[HNO_3]= 20.0 wt.% containing 25% undissociated HNO_3 (system (4)) – a detailed descritption of the system composition is available in Table S3.

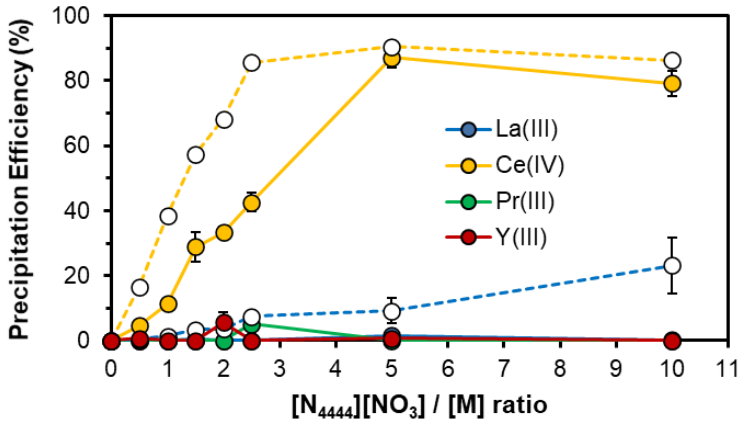

Figure S4. Precipitation efficiency (%) of REEs as a function of the [IL] to metal molar ratio at 4.5 wt.% HNO_3 (filled symbols) and 18.0 wt.% HNO_3 (empty symbols) after 24 hr agitation at 500 rpm and 293 K. All test were performed using 0.01 mol. kg of system)$^{-1}$ metal concentration.

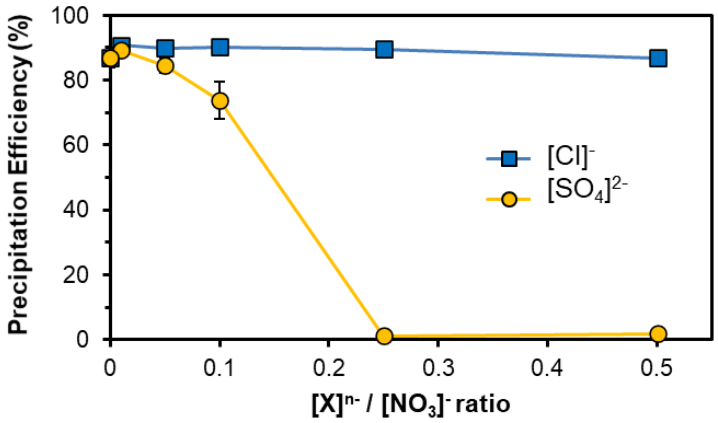

Figure S5. Precipitation efficiency (%) of 0.01 mol (kg of system)$^{-1}$ of Ce^{IV} in 4.5 wt.% HNO_3) after 24 hr agitation at 500 rpm and 293 K as a function of the anion to nitrate molar ratio in the presence of 0.10 mol (kg of system)$^{-1}$ of $[N_{4444}][NO_3]$.

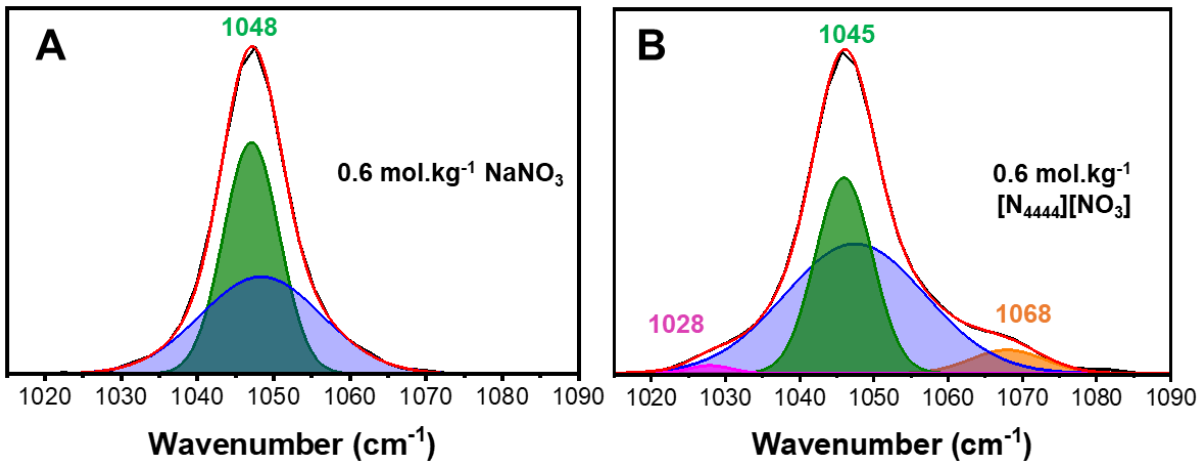

Figure S6. Deconvoluted Raman spectra of an aqueous solution of 0.6 mol kg^{-1} of A) $NaNO_3$ and B) $[N_{4444}][NO_3]$ (~20.0 wt.%). The band of free and associated nitrates are highlighted in green and magenta, respectively. Red line corresponds to the deconvoluted fit.

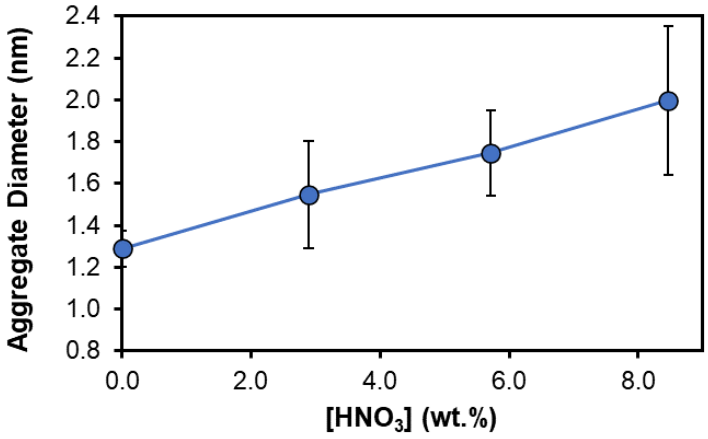

Figure S7. Average $[N_{4444}][NO_3]$ aggregate size as a function of HNO_3 concentration for a constant 20 wt.% $[N_{4444}][NO_3]$ and T= 293 K. System were very polydisperse, sample points are the average of 5 measurements over a 2 hr period.

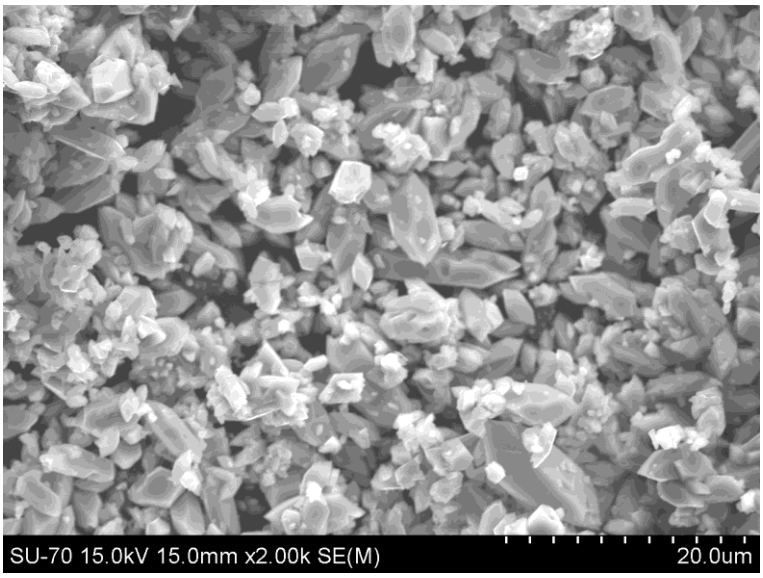

Figure S8. SEM analysis of the white precipitate obtained after pH adjustment to 1.6 of the optimised sulfuric acid NiMH black mass leachate.

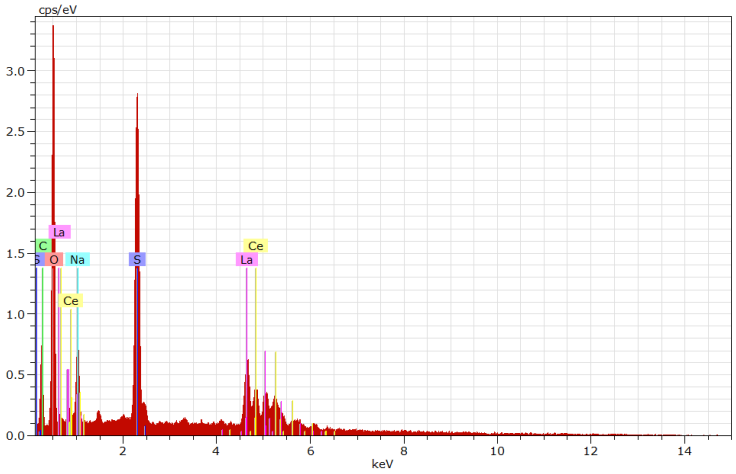

Element	Precipitate composition (wt.%)
Oxygen	28.15 ± 9.75
Carbon	12.56 ± 5.84
Sulfur	16.25 ± 1.57
Sodium	6.01 ± 1.11
Lanthanum	21.58 ± 1.78
Cerium	15.44 ± 1.34

Figure S9. EDS spectra of the recovered REE double sulfate precipitate shown in Figure S7. The presence of carbon is attributed to the sputter-coating applied to the sample to improve SEM resolution.

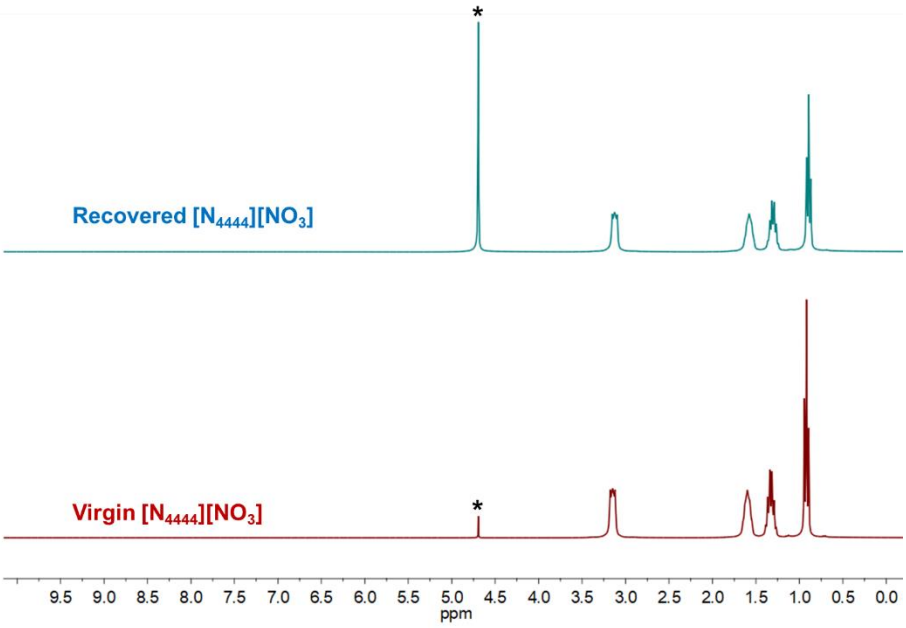

Figure S10. ^{1}H-NMR of the original and recovered $[N_{4444}][NO_3]$ after three extraction cycles. The D_2O solvent peak is highlighted by an asterix.

Tables

Table S1. Experimental binodal data for the $[N_{4444}][NO_3]$-HNO_3-H_2O systems in Figure 1A at various temperatures. All concentrations are reported in weight percent (wt.%).

293 K		303 K		313 K		323 K	
$[HNO_3]$	[IL]	$[HNO_3]$	[IL]	$[HNO_3]$	[IL]	$[HNO_3]$	[IL]
8.88	57.39	8.25	61.41	7.10	52.48	7.40	60.91
8.78	54.05	8.22	59.48	6.68	46.76	5.74	44.90
8.68	51.44	8.05	56.06	6.51	44.15	5.53	42.00
8.57	49.45	7.79	52.59	6.50	42.16	5.43	40.19
8.48	47.90	7.90	49.49	6.42	40.03	5.38	38.69
8.60	44.89	7.89	46.57	6.50	38.35	5.37	37.28
8.52	43.88	7.77	44.10	6.44	36.39	5.30	35.72
8.58	43.12	7.86	41.75	6.33	34.94	5.20	33.96
8.50	42.03	7.73	39.45	6.35	33.83	5.10	32.11
8.43	41.21	7.63	37.93	6.41	33.20	5.06	31.35
8.51	40.68	7.60	36.41	6.40	32.31	5.14	30.38
8.55	39.73	7.54	34.24	6.39	31.44	5.06	28.96
8.57	38.46	7.56	32.82	6.41	30.56	5.06	28.03
8.42	36.90	7.55	31.11	6.36	29.73	4.87	26.42
8.43	36.34	7.55	29.44	6.36	28.91	4.88	25.52
8.33	35.73	7.56	28.30	6.38	26.75	4.90	24.97
8.44	34.79	7.62	27.22	6.44	25.50	5.22	23.79
8.44	34.15	7.69	26.25	6.55	23.71	5.16	22.94
8.51	33.60	7.81	25.04	6.64	22.84	5.14	22.21
8.50	32.63	7.92	23.84	6.73	22.22	5.22	21.87
8.57	32.02	7.99	22.71	6.96	21.54	5.24	21.20
8.74	31.18	8.14	21.97	6.89	20.76	5.25	20.73
8.73	30.33	8.29	20.95	6.96	20.16	5.66	19.99
8.75	29.46	8.46	20.24	7.13	19.22	5.53	18.95
8.88	28.91	8.56	19.37	7.46	18.30	5.58	18.53
8.80	28.20	8.75	18.54	7.59	17.52	5.64	18.10
8.92	27.68	8.88	17.99	7.59	16.90	5.76	17.67
8.97	27.13	8.95	17.56	7.72	16.30	6.22	16.82
9.02	26.61	9.05	17.13	7.89	15.64	5.97	15.85
8.97	26.24	9.20	16.50	8.10	14.97	6.02	15.60
9.16	24.76	9.38	15.86	8.17	14.47	6.06	15.40
9.89	19.45	9.55	15.29	8.33	13.94	6.10	15.06
10.54	17.02	9.64	14.89	8.87	13.25	6.44	14.58

10.92	15.75	9.74	14.51	8.78	12.69	6.31	13.91
11.11	15.34	9.81	14.25	8.85	12.11	6.34	13.56
11.34	14.42	10.03	13.73	9.14	11.81	6.38	13.31
11.73	13.65	10.10	13.43	9.34	11.24	6.41	13.10
11.88	13.28	10.29	13.01	9.44	10.86	6.49	12.87
12.76	12.55	10.38	12.63	9.62	10.49	6.55	12.67
13.01	11.70	10.53	12.21	9.73	10.23	6.71	12.06
13.57	9.78	10.87	11.40	9.88	9.92	6.71	11.78
13.66	8.87	11.17	10.71	10.05	9.58	6.76	11.57
		11.49	10.09	10.20	9.30	6.83	11.44
		11.79	9.51	10.34	9.03	6.89	11.29
		12.11	8.93	10.49	8.79	6.96	11.11
		12.49	8.41	10.64	8.54	7.14	10.83
		12.65	8.10	10.75	8.32	7.14	10.59
		13.10	7.64	10.96	8.05	7.24	10.35
		13.28	7.23	11.10	7.82	7.30	10.23
				11.23	7.61	7.38	9.98
				12.18	6.44	7.54	9.79
				12.32	6.25	7.57	9.64
				12.51	6.06	7.69	9.48
				12.62	5.93	7.71	9.30
						7.74	9.20
						7.80	9.13
						7.86	8.97
						7.99	8.51
						8.20	8.25

Table S2. Experimental binodal data for the $[N_{4444}]Cl$-HNO_3-H_2O systems in Figure S1 at various temperatures. All concentrations are reported in weight percent (wt.%).

293 K		303 K		313 K		323 K	
$[HNO_3]$	[IL]	$[HNO_3]$	[IL]	$[HNO_3]$	[IL]	$[HNO_3]$	[IL]
15.48	43.59	14.16	41.87	12.94	40.46	13.09	41.43
13.93	36.14	13.33	38.89	12.38	38.15	12.48	39.61
14.00	34.09	12.40	34.70	11.59	34.91	11.98	37.09
13.72	31.49	12.05	32.46	11.31	33.17	11.36	34.49
13.46	29.25	11.73	30.92	10.79	31.02	10.96	32.23
13.53	27.71	11.49	28.72	10.64	30.04	10.84	31.30
13.51	26.32	11.38	25.99	10.40	28.90	10.60	29.91
13.49	25.08	11.06	24.68	10.32	28.06	10.29	28.74
13.48	23.98	11.16	24.01	10.14	26.83	10.11	27.88
13.36	22.78	11.06	22.83	9.95	25.67	9.96	27.02
13.42	21.97	11.06	21.67	9.81	24.74	9.96	25.62
13.62	21.16	10.86	20.62	9.68	23.99	9.43	23.67
13.66	20.35	10.88	20.25	9.79	23.35	9.31	22.46
13.53	19.47	10.89	19.81	9.76	22.67	9.22	21.43
13.77	18.84	10.88	19.33	9.69	21.96	9.08	20.32
13.89	18.34	10.89	19.02	9.70	21.14	9.02	19.56
13.87	17.73	10.91	18.33	9.65	20.56	8.95	18.79
13.94	17.20	11.05	17.30	9.65	19.94	8.91	18.00
14.01	16.80	11.02	16.49	9.63	19.21	8.90	17.19
14.03	16.36	11.07	16.02	9.61	18.77	8.89	16.47
14.08	15.93	11.09	15.62	9.69	17.61	8.85	15.28
14.26	15.65	11.12	15.40	9.66	16.74	8.88	14.69
14.41	15.38	11.21	14.83	9.79	15.64	8.91	14.26
14.78	14.96	11.26	14.43	10.02	14.70	8.96	13.55
14.81	13.63	11.29	14.07	10.01	14.07	9.03	12.98
15.21	13.08	11.36	13.71	10.11	13.70	9.06	12.45
15.66	12.51	11.34	13.38	10.23	12.84	9.08	11.75
15.38	12.01	11.38	13.15	10.31	12.34	9.19	11.23
15.51	11.86	11.46	12.90	10.41	11.71	9.27	10.81
15.64	11.34	11.49	12.58	10.52	11.24	9.37	10.35
15.82	11.09	11.52	12.35	10.61	10.89	9.48	9.92
15.90	10.89	11.52	12.19	10.76	10.33	9.54	9.77
15.92	10.72	11.64	11.92	10.93	9.81	9.61	9.51
15.95	10.51	11.63	11.52	11.10	9.33	9.76	9.10
16.00	10.34	11.67	11.25	11.17	9.04	9.91	8.72

16.11	10.21	11.72	11.07	11.35	8.62	10.17	8.10
16.10	10.05	11.84	10.83	11.51	8.23	11.62	5.68
16.15	9.89	11.91	10.47	11.82	7.64		
16.22	9.79	12.03	10.17	11.93	7.35		
16.31	9.68	12.10	9.88	12.16	7.00		
16.40	9.57	12.17	9.60	12.40	6.67		
16.52	9.47	12.33	9.33	12.86	6.05		
16.52	9.29	12.39	9.12	13.21	5.60		
16.58	9.06	12.44	8.98	13.68	5.14		
16.77	8.91	12.63	8.64				
16.78	8.79	13.06	7.77				
16.85	8.69	13.22	7.65				
16.92	8.60	13.79	6.84				
17.22	8.45	14.89	5.39				
17.31	8.35						
17.35	8.25						
17.49	8.12						
17.56	7.96						
17.88	7.78						
17.95	7.56						
17.92	7.28						
18.07	7.01						
18.10	6.88						
18.47	6.67						

Table S3. $[N_{4444}][NO_3]$ + HNO_3 + H_2O system composition for all-atom molecular dynamic simulations at 298 K as well as the final simulation box volume (V). All systems contain a fixed 200 $[N_{4444}][NO_3]$ ion pairs. Dissociated (non-protonated) HNO_3 was considered as the H_3O^+ and NO_3^- ion pair. All systems were simulated for 90 ns.

System	[IL] (wt.%)	[HNO_3] (wt.%)	n(HNO_3)	% protonated	[H_2O] (wt.%)	n(H_2O)	V (nm^3)
(1)	20.0	0.0	0	-	80.0	13532	7.86^3
(2)	20.1	4.5	216	0	75.4	12700	7.87^3
(3)	20.1	4.5	216	100	75.4	12700	7.90^3
(4)	20.1	20.0	964	25	59.9	10100	7.74^3

Table S4. Experimentally determined metal distribution coefficients (D_M) and separation factors ($SF_{Ce(IV)/M}$) in the $[N_{4444}][NO_3]$ + HNO_3 + H_2O AcABS as a function of HNO_3 concentration at T = 323 K. A constant IL and metal concentration of 20.0 wt.% and 0.01 mol (kg of system)$^{-1}$ was used respectively. Results are the average of two independent extraction tests with the associated standard deviation (σ).

[HNO_3]	$D_{Ce(IV)}$	σ	$D_{Ce(III)}$	σ	$SF_{Ce(IV)/Ce(III)}$
10.00	16.96	1.69	0.29	0.00	59.5
12.00	22.77	2.56	0.28	0.01	82.1
14.00	25.25	3.56	0.23	0.03	110.0
16.00	30.91	2.78	0.15	0.03	211.8
18.00	39.64	1.65	0.12	0.01	335.7
20.00	26.46	0.77	0.12	0.01	217.2

Table S5. Experimentally determined metal distribution coefficients (D_M) and separation factors ($SF_{Ce(IV)/M}$) in the $[N_{4444}][NO_3]$ + HNO_3 + H_2O AcABS at T = 323 K, [IL] = 20.0 wt.% and $[HNO_3]$ = 18.0 wt.% All test were performed using [M] = 0.01 mol kg^{-1} of system with the exception of [Pt] = [Au] = 2.0 mmol kg^{-1} of system. Results are the average of two independent extraction tests with the associated standard deviation (σ). * - although Sn^{II} was added, Pourbaix diagram indicates the existence of Sn^{IV} under the tested conditions.

Metal	Salt used	Purity / Supplier	D_M	σ	$\ln(SF_{Ce(IV)/M})$
Ce(IV)	$Ce(SO_4)_2.4H_2O$	98.0% / Alfa Aesar	39.6	3.3	
La(III)	$La_2(SO_4)_3.xH_2O$	99.9% Alfa Aesar	1.44×10^{-1}	3.18×10^{-3}	5.62
Ce(III)	$Ce(NO_3)_3.6H_2O$	99.9% / Fluka	1.18×10^{-1}	9.49×10^{-3}	5.82
Pr(III)	$Pr_2(SO_4)_3.8H_2O$	99.9% / Alfa Aesar	9.79×10^{-2}	7.67×10^{-3}	6.00
Nd(III)	$Nd_2(SO_4)_3.8H_2O$	99.9% / Alfa Aesar	8.88×10^{-2}	1.29×10^{-3}	6.10
Eu(III)	$Eu(NO_3)_3.5H_2O$	99.9% / Sigma Aldrich	3.73×10^{-2}	5.98×10^{-4}	6.97
Y(III)	$Y(NO_3)_3.6H_2O$	99.9% / Alfa Aesar	6.69×10^{-3}	2.30×10^{-4}	8.69
Sc(III)	$Sc_2(SO_4)_3.7H_2O$	99.9% / Sigma Aldrich	6.77×10^{-3}	1.10×10^{-3}	8.67
K(I)	KNO_3	98.0% / Panreac	1.17×10^{-3}	1.71×10^{-4}	10.43
Ca(II)	$Ca(NO_3)_2.4H_2O$	99.5% / BDH Chemicals	1.13×10^{-2}	1.18×10^{-2}	8.16
Ba(II)	$Ba(NO_3)_2$	99.9% / Alfa Aesar	2.51×10^{-3}	1.77×10^{-4}	9.67
Cr(III)	$Cr(NO_3)_3.9H_2O$	99.9% % / Sigma Aldrich	8.51×10^{-4}	6.26×10^{-4}	10.75
Mn(II)	$Mn(NO_3)_2.4H_2O$	98.5% / Merck	7.54×10^{-4}	1.39×10^{-4}	10.87
Fe(III)	$FeCl_3.6H_2O$	99.0% / Merck	1.68×10^{-2}	6.27×10^{-4}	7.77
Co(II)	$Co(NO_3)_2.6H_2O$	99.0% / Riedel de Haen	7.77×10^{-4}	8.87×10^{-5}	10.84
Ni(II)	$Ni(NO_3)_2.6H_2O$	99.0% / Riedel de Haen	1.49×10^{-3}	5.28×10^{-4}	10.19
Cu(II)	$Cu(NO_3)_2.3H_2O$	98.0% / Sigma Aldrich	6.49×10^{-3}	3.91×10^{-5}	8.72
Zn(II)	$ZnCl_2.6H_2O$	98.0% / Merck	2.63×10^{-3}	2.95×10^{-5}	9.62
Sn(II)*	$SnCl_2.2H_2O$	98.0% / Sigma Aldrich	1.88×10^{-2}	3.56×10^{-3}	7.65

Pb(II)	PbO	99.9% / Alfa Aesar	6.02×10^{-2}	1.96×10^{-3}	6.49
Ga(III)	$GaCl_3.xH_2O$	>99.9% / Acros Organics	2.37×10^{-3}	1.85×10^{-4}	9.73
In(III)	$In(NO_3)_3.H_2O$	>99.9% / Alfa Aesar	5.55×10^{-5}	0.31×10^{-5}	13.48
Bi(III)	$BiCl_3.xH_2O$	98.0% / Sigma Aldrich	30.5	2.1	0.26
Pt(IV)	$PtCl_4$	96.0% / Sigma Aldrich	1.26	0.25	3.45
Au(III)	$AuCl_3.3H_2O$	>99.9% / Sigma Aldrich	1438	887	-3.59

Table S6. Crystal data and refinement parameters of $[N_{4444}]_2[Ce^{IV}(NO_3)_6]$ as well as those for the reported $[NH_4]_2[Ce^{IV}(NO_3)_6]$

Compound	$[N_{4444}]_2[Ce^{IV}(NO_3)_6]$	$[NH_4]_2[Ce^{IV}(NO_3)_6]$
Reference	This work	[5]
a (Å)	10.4753(3)	13.061
b (Å)	19.1120(5)	6.842
c (Å)	11.7121(3)	8.183
α (deg)	90	90
β (deg)	93.4420(10)	91.34
γ (deg)	90	90
V ($Å^3$)	2340.58	731.06
Space group	P 2_1/n	P 2_1/n
Z	2	2
Dc (mg m^{-3})	1.415	-
μ/ [mm^{-1}]	1.047	-
F(000)	1044	-
Crystal size [mm^3]	0.18x0.12x0.04	-
θ range for data collection (°)	2.042-29.180	-
Index ranges	--14≤h≤11, --26≤k≤24, -16≤l≤16	-
Reflections collected	30512	-
Unique reflections, [Rint]	6319 [0.0391]	-
R1, wR2 [I>2σI]	0.0245, 0.0522 [4843]	-
R1, wR2 (all data)	0.0398, 0.0584	-
Data/restraints/ parameters	6319/0/272	-
Goodness-of-fit on F2	0.995	-

Table S7. Composition of the 2.0 mol L^{-1} H_2SO_4 leachate (mg per gram of NiMH battery black mass) and the REE double sulfate precipitate after pH adjustment to 1.6 (mg per gram of precipitate). The precipitation yields of the major element in the black mass leachate after pH adjustment are also included. Reported values are the average of three independent tests (BDL – below detection limit).

Element	Leachate composition ($mg.g^{-1}$)	Precipitate composition ($mg.g^{-1}$)	Precipitation Yield (%)
Ni	371.8 ± 1.2	BDL	≤ 0.1
Co	93.2 ± 1.2	BDL	≤ 0.1
Mn	11.9 ± 1.2	BDL	≤ 0.1
Fe	91.3 ± 1.2	BDL	≤ 0.1
La	18.8 ± 0.3	202 ± 59.3	96.5 ± 1.2
Ce	12.0 ± 0.3	139 ± 13.2	≥ 99.9
Nd	4.3 ± 0.3	59.7 ± 3.5	≥ 99.9
Pr	1.2 ± 0.3	0.91 ± 0.16	≥ 99.9

References

(1) Bruker SAINT-plus Bruker AXS Inc.,Madison, Wisconsin, USA, 2007, (n.D.).

(2) Sheldrick, G.M. (2010) SADABS, Program for Empirical Absorption Correction of Area Detector Data. University of Gottingen, Gottingen, Germany.

(3) Sheldrick, G.M., SHELX Version 2014/7, (n.D.).

(4) MacRae, C. F.; Sovago, I.; Cottrell, S. J.; Galek, P. T. A.; McCabe, P.; Pidcock, E.; Platings, M.; Shields, G. P.; Stevens, J. S.; Towler, M.; Wood, P. A. Mercury 4.0: From Visualization to Analysis, Design and Prediction. *J. Appl. Crystallogr.* **2020**, *53* (1), 226–235. https://doi.org/10.1107/S1600576719014092.

(5) Beineke, T. A.; Delgaudio, J. The Crystal Structure of Ceric Ammonium Nitrate. *Inorg. Chem.* **1968**, *7* (4), 715–721. https://doi.org/10.1021/ic50062a020.